Synthesis of Nanocrystalline $ZnFe_2O_4$ by Polymerized Complex Method for its Visible Light Photocatalytic Application: An Efficient Photo-oxidant

Jum Suk Jang,[†] Pramod H. Borse,[†,‡] Jae Sung Lee,[†] Ok-Sang Jung,[§] Chae-Ryong Cho,[#] Euh Duck Jeong,[⊥] Myoung Gyu Ha,[⊥] Mi Sook Won,[⊥] and Hyun Gyu Kim[⊥,*]

[†]*Department of Chemical Engineering, Pohang University of Science and Technology, Pohang 790-784, Korea*
[‡]*Centre for Nanomaterials, International Advanced Research Centre for Powder Metallurgy and New Materials (ARC International), Balapur PO, Hyderabad, AP, 500 005, India*
[§]*Department of Chemistry (BK21), Pusan National University, Busan 627-706, Korea*
[#]*Department of Nano Fusion Technology, Pusan National University, Miryang 627-706, Korea*
[⊥]*Busan Center, Korea Basic Science Institute, Busan 609-735, Korea. *E-mail: hhgkim@kbsi.re.kr*
Received May 19, 2009, Accepted June 16, 2009

Nanocrystalline $ZnFe_2O_4$ oxide-semiconductor with spinel structure was synthesized by the polymerized complex (PC) method and investigated for its photocatalytic and photoelectric properties. The observation of a highly pure phase and a lower crystallization temperature in $ZnFe_2O_4$ made by PC method is in total contrast to that was observed in $ZnFe_2O_4$ prepared by the conventional solid-state reaction (SSR) method. The band gap of the nanocrystalline $ZnFe_2O_4$ determined by UV-DRS was 1.90 eV (653 nm). The photocatalytic activity of $ZnFe_2O_4$ prepared by PC method as investigated by the photo-decomposition of isopropyl alcohol (IPA) under visible light ($\geq$ 420 nm) was much higher than that of the $ZnFe_2O_4$ prepared by SSR as well as $TiO_{2-x}N_x$. High photocatalytic activity of $ZnFe_2O_4$ prepared by PC method was mainly due to its surface area, crystallinity and the dispersity of platinum metal over $ZnFe_2O_4$.

Key Words: Zinc ferrites, Nano-particles, Polymerized complex method, Photocatalytic activity

Introduction

Despite several exciting and attractive developments in UV photocatalysis, the development of the visible light photocatalysts has become an important issue in the photocatalysis research today. This is because the solar spectrum contains only *ca.* 4% of UV light and *ca.* 46% of visible light. To date, many groups have developed the visible active photocatalysts of various oxides, sulfides, oxynitrides *viz.* $PbBi_2Nb_2O_9$, $(Ga_{1-x}Zn_x)(N_{1-x}O_x)$, $Ni_xIn_{1-x}TaO_4$, Zr-S co-doped TiO_2, $TiO_{2-x}N_x$, $TiO_{2-x}C_x$, and $Sm_2Ti_2O_5S_2$, *etc.*[1-8] But, we still need a low band gap (*ca.* 1.9 ~ 2.1 eV) material and a high efficiency photocatalyst so that the visible light photons from solar spectrum are efficiently utilized. N-type $ZnFe_2O_4$ with spinel structure is an attractive candidate for the visible light photo-catalysis because it has a relatively small band-gap (*ca.* 1.9 eV) necessary to absorb a larger percentage of the visible light from solar spectrum and thus is a potentially useful solar energy conversion material. Recently we observed that a photocatalyst consisting of the nanocomposites are efficient in utilization of the visible light photons as well as, in showing an unprecedented high activity for the photocatalytic oxidation of water under visible light irradiation ($\lambda \geq 420$ nm).[9-11] Thus exploring the photocatalytic activity of a single component, nanocrystalline ternary metal-oxide i.e. $ZnFe_2O_4$ alongwith its bulk counterpart is of prime importance and of a particular interest for the development of visible light active high efficiency composite photocatalyst. In recent years the polymerized complex (PC) method has been widely used to prepare the multicomponent oxides due to its uniqueness to yield an improved crystallinity and homogeneity of metal oxide at low temperature. In addition such photocatalysts have shown an enhanced photocatalytic activity.[12]

In this paper, we describe the fabrication of $ZnFe_2O_4$, *viz.* an n-type photocatalyst having a spinel structure by PC method and characterize the optical properties of the nanocrystalline $ZnFe_2O_4$ by UV-Vis diffuse reflectance spectroscopy and X-ray diffraction. We also investigated the photocatalytic and photoelectrochemical performance of the material for the photocurrent generation and the CO_2 production from the photooxidation of iso-propyl alcohol (IPA) under visible light irradiation ($\lambda \geq 420$ nm). Surprisingly the $ZnFe_2O_4$ made by PC method is much more active than the one prepared by SSR and $TiO_{2-x}N_x$.[13]

Experimental

Preparation of $ZnFe_2O_4$ nanocrystalline. Nanocrystalline $ZnFe_2O_4$ was synthesiszed by the PC method, according to the procedure described in our previous reports.[14-15] Zinc nitrate hexahydrate ($Zn(NO_3)_2 \cdot 6H_2O$, 98.0%, Aldrich), ethylene glycol ($C_2H_6O_2$, Kanto Chemicals), citric acid ($C_6H_8O_7$, Wako) and iron nitrate hydrate ($Fe(NO_3)_3 \cdot 9H_2O$, 99.99%, Aldrich) were used as starting materials. The citric acid (CA) was added into water under constant agitation, at temperature of 333 - 343 K. Next, the salts of zinc nitrate hexahydrate and iron nitrate hydrate were dissolved in citric acid-water solution to obtain the metal citrate complex. Finally, the ethylene glycol (EG) was added to the mixture to yield a mass proportion of 60% CA to 40% EG. Next, the mixture was kept on the hot plate (297 K)

till it became a transparent colorless solution. The colorless solution was then heated at 403 K for several hours to obtain a polymeric gel. The viscous polymeric product was pyrolyzed at about 573 - 773 K to form the precursor powders. Thus obtained powder was pressed in the form of pellets, which were calcined at 773 - 1473 K for 2 h in an electric furnace to obtain nanocrystalline $ZnFe_2O_4$. On the other hand, for the purpose of comparison, $ZnFe_2O_4$ was also prepared by the conventional solid-state reaction (SSR) method. Crystalline $ZnFe_2O_4$ powders were made by the heating a ground mixture of ZnO (99%, Aldrich) and Fe_2O_3 (99%, Aldrich) at various temperatures in the range of 873 - 1473 K. As an another sample for the purpose of comparison, $TiO_{2-x}N_x$ nanoparticles were also prepared by the hydrolytic synthesis method (HSM),[13] in which an aqueous ammonium hydroxide solution with an ammonia content of 28 - 30% (99.99%, Aldrich) was slowly added drop by drop to 20% titanium (III) chloride solution ($TiCl_3$, Kanto, contained 0.01% iron as the major impurity) for 30 min under N_2 flow in ice bath while continuously stirring the suspension for the next 5 h to complete the reaction. After the completion of the reaction, the precipitate was filtered in air and washed several times with deionized water. Filtered powder was dried at 343 K for 3 - 4 h in a convection oven. The sample obtained at this stage was an amorphous precipitated powder containing traces of ammonia and titanium. Further this sample was calcined at 673 K for 2 h in air flow in an electric furnace to obtain the crystalline powders of $TiO_{2-x}N_x$.

Characterization. The $ZnFe_2O_4$ samples prepared by the PC and SSR methods were characterized by X-ray Diffractometer (Mac Science Co., M18XHF). The X-ray diffraction (XRD) results were compared using the Joint Committee Powder Diffraction Standards (JCPDS) data for the phase identification. The band gap energy and the optical property of as-prepared material were studied by the UV-Visible diffuse reflectance spectrometer (Shimadzu, UV 2401). The morphology was determined by scanning electron microscopy (SEM, Hitachi, S-2460 N) and high-resolution transmission electron microscopy (HR-TEM, Philips, CM 200). The BET surface area was estimated by N_2 adsorption in a constant volume adsorption apparatus (Micrometrics, ASAP 2012).[16]

Photocatalytic reaction procedure. About 200 ppm of the gaseous iso-propyl alcohol (IPA) was injected into a 500-mL Pyrex reaction cell filled with air and 1.25 m mole of catalyst. The concentration of the reaction products (CO_2) was determined by a gas chromatograph equipped with a thermal conductivity detector and a molecular sieve 5-Å column. Before reaction, 1 wt% of Pt was deposited on the photocatalyst by using photo-deposition method under visible light ($\lambda \geq 420$ nm).

Results and Discussion

The structural characterization of the SSR and PC samples were carried out to compare their crystallization behaviors with respect to the change in the calcination temperatures. Figure 1 and 2 shows the XRD patterns of SSR and PC samples, respectively. The SSR samples calcined between 1173 and 1473 K clearly showed the peaks related to $ZnFe_2O_4$ crystal structure without other impurity phases. The formation of a spinel $ZnFe_2O_4$ structure alongwith the other impurity phases was observed in the samples calcined at 873 and 1073 K. In contrast, the growth behavior of PC samples was significantly different from that of the SSR samples as shown in Figure 2. The PC samples calcined at 773 - 973 K showed the low intensity peaks due to $ZnFe_2O_4$ crystal structure alongwith some undefined peaks, indicating that $ZnFe_2O_4$ could be crystallized at such lower temperatures. The sample calcined in the range of

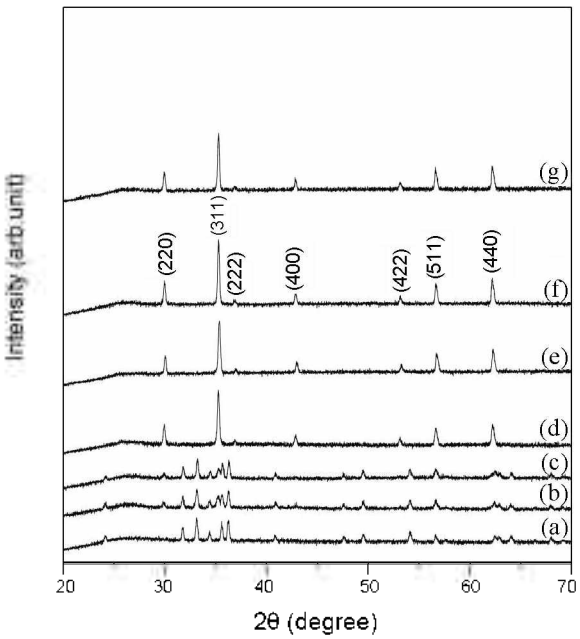

Figure 1. XRD spectra of $ZnFe_2O_4$ samples formed by the solid state reaction (SSR) calcined at (a) 873 K, (b) 973 K, (c) 1073 K, (d) 1173 K, (e) 1273 K, (f) 1373 K, (g) 1473 K, for 4 h.

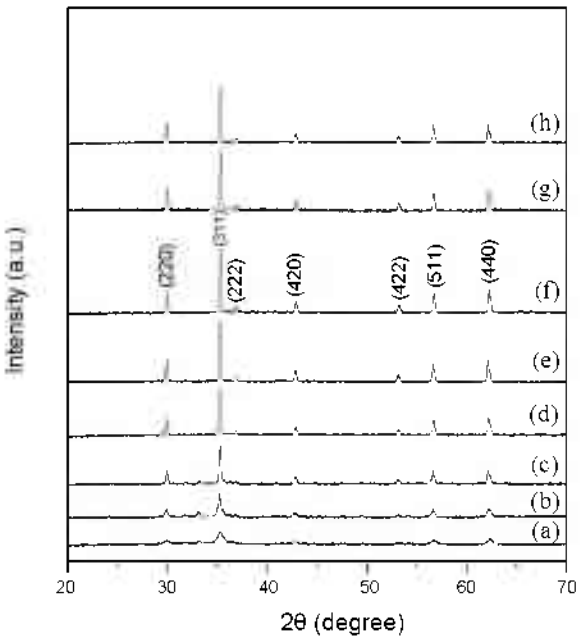

Figure 2. XRD spectra of $ZnFe_2O_4$ samples prepared by polymer complex (PC) method calcined at (a) 773 K, (b) 873 K, (c) 973 K, (d) 1073 K, (e) 1173 K, (f) 1273 K, (g) 1373 K, (h) 1473 K, for 4 h.

Table 1. Table indicating the sample made by PC/SSR method at different calcination temperatures and respective specific surface area, crystallite size and Band gap

Catalyst	Temperature (K)	BET surface area (m_2g^{-1})	Crystallite size (nm)	Band gap (eV)
$ZnFe_2O_4$-PC	973	18	48.4	1.90
$ZnFe_2O_4$-PC	1073	12	52.1	1.90
$ZnFe_2O_4$-PC	1173	9	52.9	1.90
$ZnFe_2O_4$-PC	1273	5	53.2	1.90
$ZnFe_2O_4$-PC	1373	2	53.4	1.90
$ZnFe_2O_4$-PC	1473	-	53.5	1.90
$TiO_{2-x}N_x$	673	46	13.2	2.76
$ZnFe_2O_4$-SSR	1173	4	51.9	1.90
$ZnFe_2O_4$-SSR	1273	1	52.5	1.90
$ZnFe_2O_4$-SSR	1373	1	53.0	1.90
$ZnFe_2O_4$-SSR	1473	-	53.4	1.90

1073 - 1473 K exhibited a single phase of $ZnFe_2O_4$ without any impurity phases. These results indicate that the crystal phase in the $ZnFe_2O_4$ prepared by PC method formed at a lower temperature than that of the $ZnFe_2O_4$ prepared by SSR method.

As shown in Table 1, the crystallite sizes of the $ZnFe_2O_4$ formed by SSR sample (e) and PC sample (g), were estimated from the FWHM of main XRD peak (see Figs. 1 (g) and 2 (f)) by using the Scherrer's equation:[17]

$$D = 0.9\lambda / B\cos\theta \quad (1)$$

where λ is the wavelength of the X-ray radiation ($\lambda = 0.154$ nm), B is FWHM of the peak (in radians) corrected for instrumental broadening, θ is Bragg angle, and D is the crystallite size (Å). Table 1 summarizes the results of the respective crystallite size and their BET surface areas for the PC and the SSR samples calcined at different temperatures. The crystallite sizes of $ZnFe_2O_4$ particles prepared in both the cases show a trend of increase in size with the increasing calcination temperature. However all the samples exhibiting spinel phase on an average show the similar crystallite size (*ca.* 52 ~ 53 nm). In the case of lower calcination temperatures (< 1273 K), the surface area of $ZnFe_2O_4$ prepared by PC method was higher than those of the $ZnFe_2O_4$ prepared by SSR method. This is the outcome of the growth of several nuclei in a chemical methodology. The crystallite size and BET surface area in both PC and SSR samples prepared at high calcination temperatures (> 1273 K) were similar, due to complete densification.

Figure 3 compares the SEM images of $ZnFe_2O_4$ crystals prepared by the SSR method (A) and PC method (B). Both the samples consist of the fine particles in the size range of 3 - 10 μm. These particles are constituted of several nanocrystals of 53.4 nm/53.0 nm as estimated by using Scherrer's equation. Despite the similarity in the crystallite sizes, it is seen that the average particle size for $ZnFe_2O_4$ formed in the PC sample is smaller and the morphology is relatively more diverse compared to those formed in the SSR sample, which yields high surface area in case of sample made by PC method.

Figure 4 shows UV-Vis diffuse reflectance spectra for SSR and the PC sample calcined at 1273 K, alongwith that of $TiO_{2-x}N_x$.

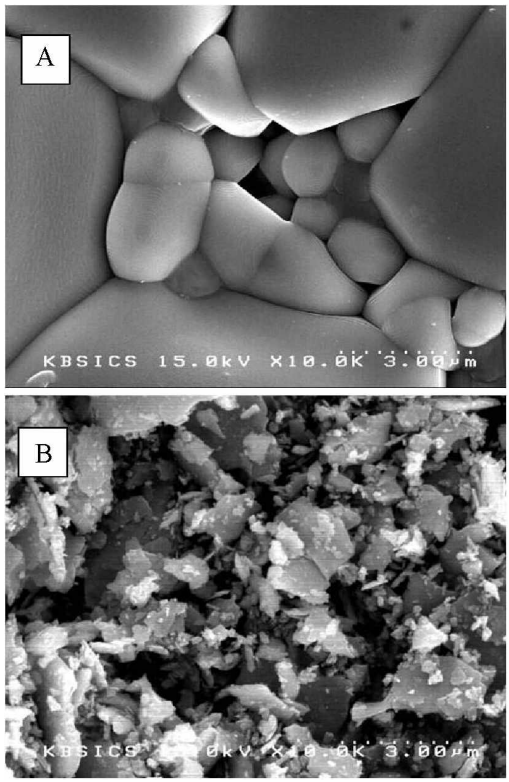

Figure 3. SEM images of $ZnFe_2O_4$ prepared by (A) SSR and (B) PC method. The samples were calcined at 1173 K for 4 h in both cases.

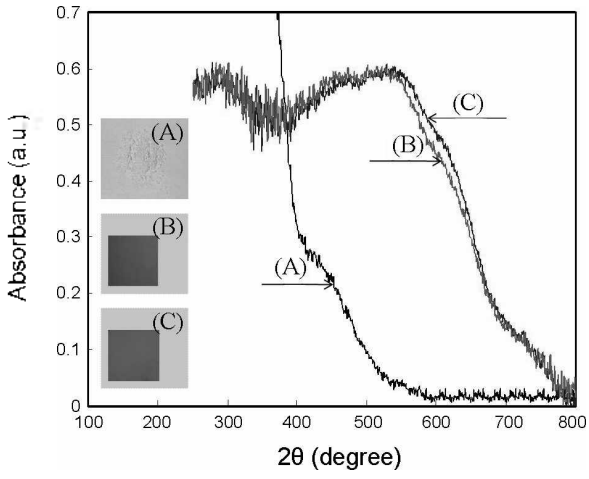

Figure 4. UV-Vis diffuse reflectance spectra of (A) $TiO_{2-x}N_x$, (B) $ZnFe_2O_4$-SSR and (C) $ZnFe_2O_4$-PC. SSR and PC samples were calcined at 1273 K for 4 h. The inset of Figure 4 shows the color of as-synthesized samples.

From these spectra, we estimated the band gap energy of these materials as summarized in Table 1. The $ZnFe_2O_4$ prepared by SSR and PC method showed a sharp edge, while $TiO_{2-x}N_x$ showed two absorption edges: the main edge due to the oxide at 390 nm and a shoulder due to the nitride at 451 nm.[1] The colors of these materials were dark brown and yellow indicating that these materials could indeed absorb the visible light and thus are suitable for the role of visible light photocatalyst. The band gaps estimated from the UV-Vis spectra of $ZnFe_2O_4$

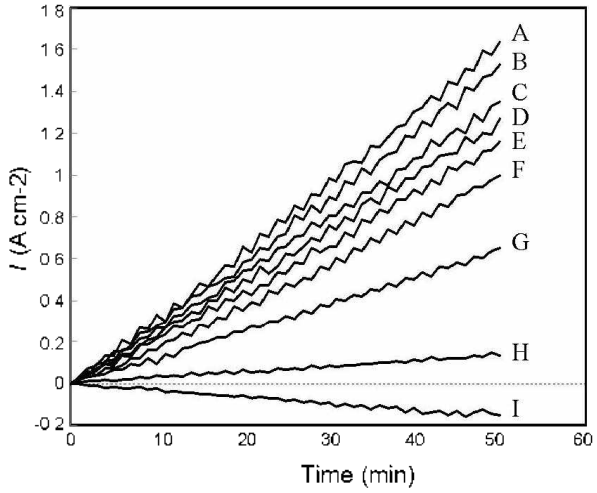

Figure 5. The generated photocurrents under visible light ($\lambda \geq 420$ nm) irradiation for $TiO_{2-x}N_x$ and $ZnFe_2O_4$ material suspensions with acetate and Fe^{3+}, as an electron donor or acceptor, respectively. Experimental conditions: photocatalysts = 0.025 g / 75 ml ; acetate = 0.1 M; Fe^{3+} – 0.1 mM; continuous N_2 purging; pH – 1.4; E_{app} – 0.6 V (vs SCE); Pt plate (10 × 10 × 0.125 mm), Pt-gauze as working and counter electrodes respectively. (A) PC-1273 K, (B) PC-1373 K, (C) SSR-1373 K, (D) PC-1473 K, (E) SSR-1473 K, (F) SSR-1273 K, (G) $TiO_{2-x}N_x$, (H) PC-1173 K, (I) TiO_2. The $ZnFe_2O_4$ sample names denote the corresponding method of preparation (SSR/PC) and calcination temperature.

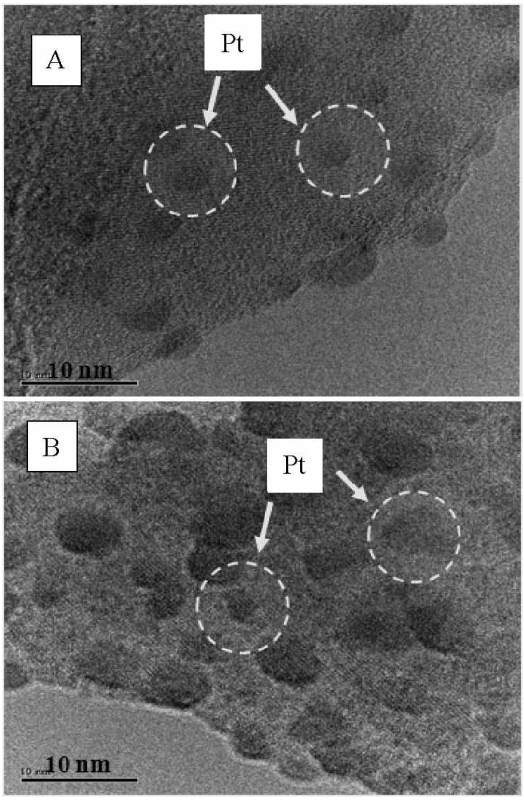

Figure 6. HR-TEM images of a 1wt% platinum-loaded $ZnFe_2O_4$ made by (A) SSR and (B) PC method. The Pt was deposited on photocatalysts by photodeposition method under visible light ($\lambda \geq 420$ nm). The $ZnFe_2O_4$ SSR was prepared by calcination at 1373 K for 4 h.

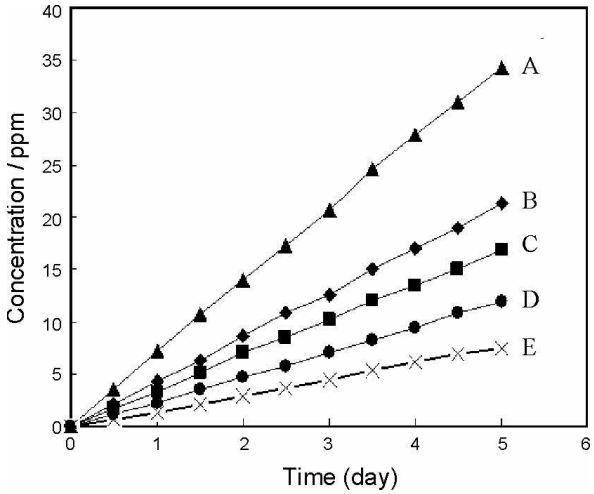

Figure 7. Time courses of CO_2 evolution from IPA decomposition over different samples under visible light irradiation ($\lambda \geq 420$ nm) in presence of 1 g photocatalyst viz. (A) PC-1273 K, (B) PC-1373 K, (C) SSR-1373 K, (D) SSR-1273 K, (E) $TiO_{2-x}N_x$; IPA concentration, 200 ppm in air. The $ZnFe_2O_4$ sample names denote the corresponding method of preparation (SSR/PC) and calcination temperature.

prepared by SSR/PC method and $TiO_{2-x}N_x$ are 1.90 eV and 2.76 eV, respectively.

Visible light active photocatalysts should generate photocurrents upon absorption of the photons. To investigate the photocurrent generation, aqueous suspensions of the materials containing acetate (donor) and Fe^{3+} (acceptor) were illuminated with visible light ($\lambda \geq 420$ nm). Figure 5 shows the photocurrents generated over $TiO_{2-x}N_x$ and $ZnFe_2O_4$ samples prepared by SSR and PC method and calcined at different temperatures. Unmodified TiO_2 with a wide band gap (3.2 eV) under irradiation, as well as all other catalysts in the dark did not generate any photocurrent as expected. At same calcination temperature the photocurrent of all samples prepared by PC method represents higher than that of samples prepared by SSR method. PC sample calcined at 1273 K generated photocurrent approximately 2 times higher than SSR sample calcined at 1273 K and 15 times faster than $TiO_{2-x}N_x$ sample. The generation of photocurrent means the critical initial step of photocatalytic reactions upon light irradiation, and the current value can be directly correlated with the photocatalytic activity of the material.

Prior to the photocatalytic studies, we loaded the platinum nanoparticles on $ZnFe_2O_4$ samples (SSR and PC) calcined at different temperatures, using the photodeposition method.[18] Figure 6 shows the HR-TEM images of 1 wt% platinum-loaded $ZnFe_2O_4$ samples made by (A) SSR and (B) PC method. In both case we observe a well dispersed platinum (3 ~ 4 nm) nanoparticles on the $ZnFe_2O_4$ particle surface. Interestingly, the platinum nanoparticles over $ZnFe_2O_4$ prepared by PC (B) method exhibit a better distribution over the significantly larger surface area than that on the $ZnFe_2O_4$ prepared by SSR method (A).

We performed the photo-oxidation reaction of iso-propyl alcohol (IPA) as a common model compound to evaluate the photodegradation capability of photocatalysts over as-prepared samples under visible light ($\lambda \geq 420$ nm). Figure 7 shows the time curves of CO_2 evolution from the photo decomposition

of IPA. In all cases, the concentration of CO_2 evolved increased steadily with the irradiation time and no intermediate reaction products were detected (not shown here). The superiority of the $ZnFe_2O_4$ prepared by PC method, as expected from the photocurrent studies, was evident and thus confirmed. Thus the nanocrystalline $ZnFe_2O_4$ can be considered as an active component of a composite photocatalyst for decomposition of water, toxic or hazard gases under visible light irradiation.

Conclusions

Spinel-type zinc ferrite material, $ZnFe_2O_4$, with high crystallinity, high surface area and homogeneity has been successfully synthesized by polymer complex method. The crystal phase of $ZnFe_2O_4$ can be achieved at a lower temperature by the PC method than by SSR method. The visible light IPA photo-degradation activity of nanocrystalline $ZnFe_2O_4$ prepared by PC method is much higher than that prepared by SSR method as well as to that of $TiO_{2-x}N_x$. Thus the spinel structured nanocrystalline $ZnFe_2O_4$ prepared by polymerized complex method can be used as an efficient photocatalyst for the decomposition of a toxic or hazard gases under the visible light irradiation.

Acknowledgments. This work has been supported by KBSI grant T29320, MKE-RTI04-0201, KOSEF grant (NCRCP, R15-2006-022-01002-0), Hydrogen Energy R&D Center, Korea.

Reference

1. Kim, H. G.; Hwang, D. W.; Lee, J. S. *J. Am. Chem. Soc.* **2004**, *126*, 8913.
2. Maeda, K.; Takata, T.; Hara, M.; Saito, N.; Inoue, Y.; Kobayashi, H.; Domen, K. *J. Am. Chem. Soc.* **2005**, *127*, 8286.
3. Zou, Z.; Ye, J.; Sayama, K.; Arakawa, H. *Nature* **2002**, *424*, 625.
4. Kim, S. W.; Khan, R.; Kim, T. J.; Kim, W. *Bull. Korean Chem. Soc.* **2008**, *29*, 1217.
5. Asahi, R.; Ohwaki, T.; Aoki, K.; Taga, Y. *Science* **2001**, *293*, 269.
6. Khan, S. U. M.; Al-Shahry, M.; Ingler, W. B., Jr. *Science* **2002**, *297*, 2243.
7. Sakthivel, S.; Kisch, H. *Angew. Chem. Int. Ed.* **2003**, *42*, 4908.
8. Subramanian, E.; Baeg, J.; Kale, B. B.; Lee, S. M.; Moon, S.; Kong, K. *Bull. Korean Chem. Soc.* **2007**, *28*, 2089.
9. Kim, H. G.; Borse, P. H.; Choi, W.; Lee, J. S. *Angew. Chem. Int. Ed.* **2005**, *44*, 4585.
10. Kim, H. G.; Jeong, E. D.; Borse, P. H.; Jeon, S.; Yong, K. J.; Lee, J. S.; Li, W.; Oh, S. H. *Appl. Phys. Letts.* **2006**, *89*, 064103.
11. Jang, J. S.; Hwang, D. W.; Lee, J. S. *Catal. Today* **2007**, *120*, 174.
12. Ikeda, S.; Hara, M.; Kondo, J. N.; Domen, K. *Chem. Mater.* **1998**, *10*, 72.
13. Jang, J. S.; Kim, H. G.; Ji, S. M.; Bae, S. W.; Jung, J. H.; Shon, B. H.; Lee, J. S. *J. Solid State Chem.* **2006**, *179*, 1067.
14. Kim, H. G.; Hwang, D. W.; Bae, S. W.; Jung, J. H.; Lee, J. S. *Catal. Lett.* **2003**, *91*, 193.
15. Jung, E. D.; Borse, P. H.; Jang, J. S.; Lee, J. S.; Cho, C. R.; Bae, J. S.; Park, S.; Jung, O. S.; Ryu, S. M.; Won, M. S.; Kim, H. G. *J. Nanosci. Nanotech.* **2009**, *9*, 3568.
16. Khan, R.; Kim, S. W.; Kim, T.; Lee, H. *Bull. Korean Chem. Soc.* **2007**, *28*, 1951.
17. Cullity, B. D. *Elements of X-ray Diffraction*, 2nd Ed; Addison-Wesley Publishing Company, Inc.: Reading, MA 1978.
18. Lee, J.; Choi, W. *J. Phys. Chem. B* **2005**, *109*, 7399.